

# Speeding Up Squeezing with a Periodically Driven Dicke Model

Jarrod T. Reilly,<sup>1</sup> Simon B. Jäger,<sup>2</sup> John Drew Wilson,<sup>1</sup> John Cooper,<sup>1</sup> Sebastian Eggert,<sup>2</sup> and Murray J. Holland<sup>1</sup>

<sup>1</sup>*JILA, NIST, and Department of Physics, University of Colorado, 440 UCB, Boulder, CO 80309, USA*

<sup>2</sup>*Physics Department and Research Center OPTIMAS, University of Kaiserslautern-Landau, D-67663, Kaiserslautern, Germany*

(Dated: October 12, 2023)

We present a simple and effective method to create highly entangled spin states on a faster timescale than that of the commonly employed one-axis twisting (OAT) model. We demonstrate that by periodically driving the Dicke Hamiltonian at a resonance frequency, the system effectively becomes a two-axis countertwisting Hamiltonian which is known to quickly create Heisenberg limit scaled entangled states. For these states we show that simple quadrature measurements can saturate the ultimate precision limit for parameter estimation determined by the quantum Cramér-Rao bound. An example experimental realization of the periodically driven scheme is discussed with the potential to quickly generate momentum entanglement in a recently described experimental vertical cavity system. We analyze effects of collective dissipation in this vertical cavity system and find that our squeezing protocol can be more robust than the previous realization of OAT.

*Introduction.*— For centuries, advancements in precision measurements have continuously propelled the scientific community’s understanding of the fundamental nature of reality. This inspired both the quantum revolution and Einstein’s theories of relativity, with the frontier of each still advancing through the use of increasingly precise experiments [1–5]. Current state-of-the-art precision measurements can detect a change of mirror distance of  $10^{-3}$  of the proton’s width in gravitational wave detectors [5–7] and have led to the development of atomic clocks with a fractional frequency uncertainty of  $10^{-21}$  [8], among many other groundbreaking achievements [9–17].

Most precision metrology experiments still operate at or above the standard quantum limit (SQL), which is the fundamental sensitivity threshold that arises from shot noise in measurements of uncorrelated quantum states. This limit on product states can be overcome through the use of entangled quantum states, and if this can be consistently utilized, it would revolutionize precision measurements with the potential to discover new physics. Although there have been proof of principle experimental demonstrations of quantum entanglement, applications for a true sensing purpose have so far been limited [18–22]. For example, spin squeezing offers a promising platform to perform atomic clock experiments beyond the SQL, but often require a long squeezing time during which quantum correlations may be destroyed by decoherence.

In this Letter, we propose an experimentally relevant scheme to realize spin squeezing in a short propagation time. We show that driving the Dicke model [23–28] at a parametric resonance leads to an effective two-axis countertwisting (TACT) Hamiltonian which can reach Heisenberg limited scaling in a shorter timescale than the commonly employed one-axis twisting (OAT) Hamiltonian. While the TACT Hamiltonian has been studied theoretically [29–42], it has so far been elusive to achieve

experimentally. We demonstrate how TACT may be realized in a current, state-of-the-art vertical cavity experiment [43–46] by periodically modulating an injected field that drives the cavity. We discuss how to make optimal use of the system’s entanglement for phase estimation using a recent advance that uncovers a state’s full metrological potential by diagonalizing the quantum Fisher information matrix (QFIM) [47]. We then perform a Bayesian phase reconstruction sequence where, remarkably, we find that simple quadrature measurements saturate the quantum Cramér-Rao bound (QCRB) [48].

*Periodically Driven Dicke Model.*— We consider  $N$  atoms that are collectively coupled through a cavity field. The atoms have ground state  $|\downarrow\rangle$  and excited state  $|\uparrow\rangle$ , and we define the collective raising and lowering operators  $\hat{J}_+ = \sum_j |\uparrow\rangle_j \langle\downarrow|_j = \hat{J}_+^\dagger$ . This system has an underlying  $SU(2)$  symmetry with basis operators  $\hat{J}_x = (\hat{J}_+ + \hat{J}_-)/2$ ,  $\hat{J}_y = i(\hat{J}_- - \hat{J}_+)/2$ , and  $\hat{J}_z = [\hat{J}_+, \hat{J}_-]/2$ , as well as the quadratic Casimir operator  $\hat{J}^2 = \hat{J}_x^2 + \hat{J}_y^2 + \hat{J}_z^2$ . After eliminating the cavity in the dispersive regime, we consider dynamics governed by the time-dependant Dicke Hamiltonian [49]

$$\hat{H} = \hbar\Delta\hat{J}_z + \hbar\chi\cos(\omega t)\hat{J}_x^2, \quad (1)$$

where  $\Delta$  is a detuning and  $\chi$  scales the cavity-mediated nonlinearity. This Hamiltonian can model, for example, Raman transitions between hyperfine states using two time-dependent transverse fields [26, 27]. For now, we ignore cavity decay based on large cavity detuning, such that the dynamics are governed by the Schrödinger equation  $\partial_t\hat{\rho} = -i[\hat{H}, \hat{\rho}]/\hbar$  with density matrix  $\hat{\rho}$ . We discuss the effects of non-negligible dissipation in the next section.

The nonlinearity in Eq. (1) creates an entangled state which can be used to sense a physical parameter with a quantum advantage. To find the parameter  $\Phi$  that the generated state is most sensitive to, one finds the maximum quantum Fisher information (QFI),  $\lambda_{\max}$ , by

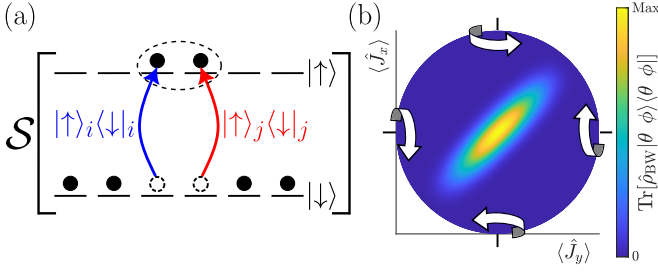


FIG. 1. (a) Schematic of the pair production process  $\hat{J}_+^2$  that the PDD model drives (along with  $\hat{J}_-^2$ ) to generate interparticle entanglement (dashed line). Here,  $\mathcal{S}$  is the symmetrizer which sums over all permutations of  $i$  and  $j$  [52]. (b) The collective Bloch sphere for  $\hat{\rho}_{\text{BW}}$  in the rotating frame of Eq. (4). The color represents the state's overlap with the coherent spin state  $|\downarrow, \phi\rangle = \exp[-i\phi\hat{J}_z] \exp[-i\theta\hat{J}_y] |\downarrow\rangle^{\otimes N}$  at each point. The arrows indicate the direction of twisting about each axis.

calculating the largest eigenvalue of the quantum Fisher information matrix (QFIM) [47],

$$\mathcal{F}\vec{\mathcal{O}} = \lambda_{\text{max}}\vec{\mathcal{O}}, \quad (2)$$

where the elements of the QFIM are given by [50]

$$\mathcal{F}_{\mu\nu} = \sum_{i,j=0;\varrho_i+\varrho_j\neq 0}^{\dim[\hat{\rho}]-1} \frac{2 \text{Re} \left[ \langle \varrho_i | [\hat{J}_\mu, \hat{\rho}] | \varrho_j \rangle \langle \varrho_j | [\hat{\rho}, \hat{J}_\nu] | \varrho_i \rangle \right]}{\varrho_i + \varrho_j}, \quad (3)$$

with  $\mu, \nu \in \{x, y, z\}$  and the spectral decomposition  $\hat{\rho} = \sum_i \varrho_i |\varrho_i\rangle\langle\varrho_i|$ . The eigenvector  $\vec{\mathcal{O}}$  associated with this maximum eigenvalue corresponds to the generator  $\hat{\mathcal{G}}$  that encodes the optimal parameter [47],  $\exp[-i\hat{\mathcal{G}}\Phi]$ . The QFI for unentangled states can reach the SQL,  $\lambda_{\text{max}} = N$ , while entangled states can reach the Heisenberg limit (HL),  $\lambda_{\text{max}} = N^2$ , which is the fundamental limit on sensing set by the Heisenberg uncertainty principle [51].

Although we will use Eq. (1) for our numerical simulations, one can gain a better intuition of the dynamics by transforming into a rotating frame. We move into an interaction picture  $\tilde{\rho} = \hat{U}^\dagger \hat{\rho} \hat{U}$  with  $\hat{U} = \exp[-i\Delta\hat{J}_z]$ , so that Eq. (1) becomes

$$\tilde{H} = \frac{\hbar\chi}{4} \cos(\omega t) \left[ e^{2i\Delta t} \hat{J}_+^2 + 2 \left( \hat{J}_+ \hat{J}_- - \hat{J}_z \right) + e^{-2i\Delta t} \hat{J}_-^2 \right]. \quad (4)$$

In the majority of previous work, one assumes a constant nonlinear interaction rate  $\omega = 0$ . Then, in the limit  $|\Delta| \gg N|\chi|$ , one makes the rotating-wave approximation (RWA) [53] to drop the fast-oscillating  $\hat{J}_\pm^2$  terms. We now explore an opposite regime in which the system is instead driven on the special resonance  $\omega = 2\Delta$ . Equation (4) after the RWA becomes

$$\hat{H}_{\text{PDD}} \approx \frac{\hbar\chi}{8} \left( \hat{J}_+^2 + \hat{J}_-^2 \right), \quad (5)$$

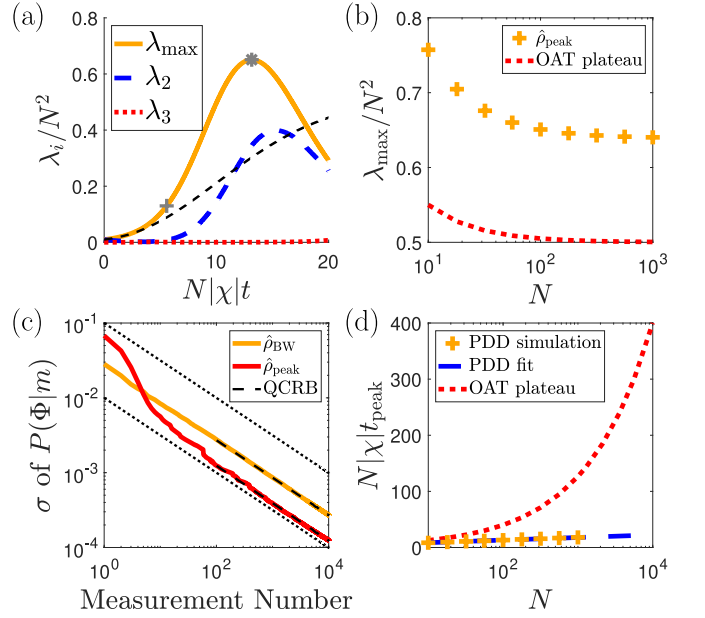


FIG. 2. (a) The three eigenvalues of the QFIM  $\mathcal{F}$  for  $N = 100$ . The state evolves under Eq. (1) with  $\Delta = 100N|\chi|$ . The gray plus and asterisk indicate when the system reaches  $\hat{\rho}_{\text{BW}}$  and  $\hat{\rho}_{\text{peak}}$ , respectively. Also shown is the largest eigenvalue of the QFIM for OAT with the same parameters (dashed black line). (b) The largest QFIM eigenvalue for  $\hat{\rho}_{\text{peak}}$ . Also shown is the plateau value of  $N(N+1)/2$  for OAT. (c) Sensitivity, given by the standard deviation  $\sigma$  of the posterior distribution for the optimal parameter  $\Phi$  after applying Bayes theorem. We display results for the states  $\hat{\rho}_{\text{BW}}$  and  $\hat{\rho}_{\text{peak}}$ , and the dashed lines represent the QCRB for the respective state. The top and bottom dotted lines represent the SQL and HL, respectively. (d) Comparing the time of maximum QFI for PDD  $t_{\text{peak}}$  (orange plus) with the time OAT reaches its plateau  $t_{\text{pl}}$  (dotted red line) for a constant  $N|\chi|$ . We also show the curve fit of the PDD simulations given by Eq. (7) (dashed blue line).

which is seen by expanding  $\cos(\omega t) = (\exp[i\omega t] + \exp[-i\omega t])/2$ . We label this as the periodically driven Dicke (PDD) model and note that it is reminiscent of two-axis countertwisting (TACT) [29], which was found to reach HL scaling on an exponential timescale [31, 35] through the pair production and twisting processes shown in Fig. 1. Beginning in the collective ground state  $\hat{\rho}_0 = |\downarrow\rangle\langle\downarrow|^{\otimes N}$ , we examine the sensitivity of the PDD model using the maximum QFI from Eq. (2). We display the dynamics of the QFIM eigenvalues in Fig. 2(a) for the case of  $N = 100$ . Here, one can see the exponential scaling of the maximum QFI on short timescales. In the rotating frame of Eq. (4), we find that the optimal generator corresponding to  $\lambda_{\text{max}}$  is given by  $\hat{\mathcal{G}} = (\hat{J}_x + \hat{J}_y)/\sqrt{2}$ . This can be understood by interpreting Eq. (5) as an analog to the photonic Kerr nonlinearity [54] which can be formalized if one performs the Holstein-Primakoff approximation assuming low atomic excitations [55, 56].

During the initial squeezing, the state can be rotated to have a high overlap with the Berry-Wiseman (BW)

phase state [57] which we label as  $\hat{\rho}_{\text{BW}}$  and display in Fig. 1(b). This state maximizes the information gained about an unknown phase after a single measurement [58] and has a full  $2\pi$  dynamic range (see Supplemental Material (SM) [59]). The fidelity with the phase state reaches unity [35], which occurs at  $t \approx 5.57/(N|\chi|)$  for  $N = 100$ . As the system continues to squeeze, it reaches the state  $\hat{\rho}_{\text{peak}}$  which maximizes the QFI in time. Here, the system is HL scaled with  $\lambda_{\text{max}} \sim 0.65N^2$ , and we discuss interesting properties of this state in the SM [59]. In the large  $N$  limit, we find that the maximum QFI asymptotes to  $\lambda_{\text{max}} \sim 0.64N^2$ , as shown in Fig. 2(b). One can then rotate  $\hat{\rho}_{\text{peak}}$  to make a specific operator the optimal generator in order to exploit the largest amount of intra-particle entanglement for a specific sensing purpose [47]. For example, in atomic clock systems, one would perform a  $\pi/2$  pulse about  $(\hat{J}_x - \hat{J}_y)/\sqrt{2}$  in the rotating frame to make  $\hat{J}_z$  the optimal generator.

While the PDD model can clearly reach a high QFI on an exponentially short timescale, the QCRB is not guaranteed to be achievable with experimentally accessible measurements. This is because the QFI implicitly optimizes over all measurement bases [50]. Remarkably, the system saturates the QCRB with simple population measurements by performing a Bayesian reconstruction protocol. To demonstrate this, we first rotate the state by a  $\pi/2$  pulse with the optimal generator  $\hat{\mathcal{G}}$  such that its anti-squeezed axis is parallel with the equator of the Bloch sphere. We encode the parameter  $\Phi$  using  $\hat{\mathcal{G}}$  and implement Bayes theorem  $P(\Phi|m) = P(m|\Phi)P(\Phi)/P(m)$ , where  $P(\Phi|m)$  is a conditional probability for the outcome  $m$  of a  $\hat{J}_z$  measurement. We begin the process with a flat prior  $P(m|\Phi) = \text{const.}$ , which we then consistently update using the posterior distribution  $P(\Phi|m)$  [60].

Figure 2(c) displays the sensitivity of the posterior distribution for the states  $\hat{\rho}_{\text{BW}}$  and  $\hat{\rho}_{\text{peak}}$  after the rotation to the Bloch sphere's equator. We also show the SQL and HL as the upper and lower dotted lines, and remarkably, the sensitivity of  $\hat{\rho}_{\text{peak}}$  nearly reaches the HL. After  $M$  measurements, the respective QCRBs are given by  $1/\sqrt{M\lambda_{\text{max}}(t)}$ , which we plot as dashed lines. In both cases, the standard deviation  $\sigma$  of the posterior distribution  $P(\Phi|m)$  saturates this bound when  $M \gtrsim 100$ , showing that simple quadrature measurements are optimal for the generated states. We can calculate the decibel gain over the SQL,  $G = 10 \log_{10}(\sqrt{\lambda_{\text{max}}/N})$ , and obtain  $G = 5.7 \text{ dB}$  and  $G = 9.1 \text{ dB}$  of squeezing for  $\hat{\rho}_{\text{BW}}$  and  $\hat{\rho}_{\text{peak}}$ , respectively. For  $\hat{\rho}_{\text{peak}}$  in the large  $N$  limit, we expect the gain to scale as  $G \approx 5 \log_{10}(N) - 1$ .

As a means for comparison, we now consider  $\omega = 0$  in Eq. (1) and eliminate the fast-oscillating  $\hat{J}_{\pm}^2$  terms via the RWA. This gives the one-axis twisting (OAT) Hamiltonian [29],

$$\hat{H}_{\text{OAT}} \approx -\frac{\hbar\chi}{2} \hat{J}_z^2, \quad (6)$$

as exploited in Refs. [44, 45]. Here, we have used the relation  $\hat{J}_+ \hat{J}_- = \hat{J}^2 - \hat{J}_z^2 + \hat{J}_z$  and ignored a constant energy shift of  $N(N/2 + 1)/2$  from the  $\hat{J}^2$  term since we remain in the collective subspace  $\{|j = N/2, m\rangle, -j \leq m \leq j\}$ .

When the state begins in an eigenvector of  $\hat{J}_x$ ,  $\hat{\rho}_0 = [(|\uparrow\rangle + |\downarrow\rangle)(\langle\uparrow| + \langle\downarrow|)/2]^{\otimes N}$ , the OAT Hamiltonian reaches  $\lambda_{\text{max}} = N(N + 1)/2$  on a timescale of  $t_{\text{pl}} \sim 4/(\sqrt{N}|\chi|)$  [47, 48, 61]. We show this initial behavior of the maximum QFI for OAT as a dashed black line in Fig. 2(a). The QFI then remains at this value for a long plateau before eventually growing again at  $t_{\text{pl},f} \sim \pi/|\chi| - 4/(\sqrt{N}|\chi|)$  [47, 48, 61]. For typical parameters, this is often too long of a timescale since decoherence will significantly reduce the squeezing performance. We compare the typical timescales for HL scaling of PDD and OAT in Fig. 2(d). We find that the PDD model indeed scales on a much faster timescale, an observation which becomes more pronounced if one considers larger atom numbers. Fitting the scaling of the PDD model, we find that the time that QFI is maximized is given by

$$t_{\text{peak}} \approx [\ln(N^2) + 4]/(N|\chi|), \quad (7)$$

which approximately matches the analysis of Ref. [31] with the Wineland squeezing parameter. Therefore, the PDD model is a full order of magnitude faster than OAT when one scales up to  $N = 10^4$  while reaching a higher QFI, as shown in Figs. 2(b) and 2(d). Moreover, the states created by OAT do not, in general, saturate the QCRB using simple quadrature measurements when encoding the optimal parameter  $\Phi$ .

*Example Experimental Realization.*— Having established that the PDD model can outperform OAT on short timescales, we now turn to a prototypical experimental realization of this scheme. For this, we consider momentum squeezing in a recent vertical cavity (VC) experiment [43–46], shown schematically in Fig. 3(a). Details of the theoretical analysis of this setup are given in the SM [59], and we describe the general features below. A packet of  $N$   $^{87}\text{Rb}$  atoms fall through an optical mode of a VC under the influence of gravity  $\vec{g} = -g\vec{e}_z$  with unit vector  $\vec{e}_z$  along the vertical axis. The cavity decays at an intensity decay rate  $\kappa$ , while an injected field pumps the VC at a rate  $\eta$ . The atoms undergo Bragg transitions on the  $D_2$  cycling transition  $|F = 2, m_F = 2\rangle \leftrightarrow |F' = 3, m_{F'} = 3\rangle$  when the detuning between the cavity mode and atomic transition frequency is large. In this regime, the excited state  $|F' = 3, m_{F'} = 3\rangle$  can be adiabatically eliminated [45, 59] such that we can focus solely on the external degrees of freedom of the atoms.

The atoms are prepared with high overlap with the momentum ground state  $|0\hbar k\rangle$ . By letting the atomic packet fall for a sufficient time  $\tau$  before turning on the injected field, the momentum states  $|0\hbar k\rangle$  and  $|2\hbar k\rangle$  become nearly degenerate in the co-falling reference frame [45]. This allows one to drive Bragg transitions

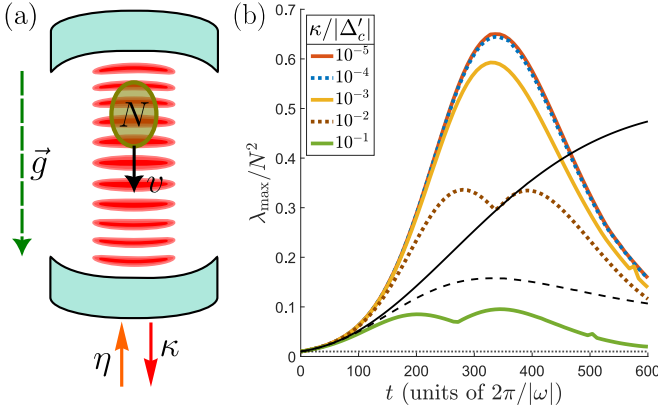


FIG. 3. (a) A schematic of the vertical cavity experiment of Refs. [43, 44]. (b) The largest eigenvalue of the QFI for the VC setup with different decay rates. The simulations evolve under Eq. (12) with the full Hamiltonian of Eq. (8). We choose the parameters  $N = 100$ ,  $|\Delta'_c| = 10.5|\omega_g|$ ,  $|U_0| = 5.1|\omega_g| \times 10^{-3}$ , and  $|\beta_0| = 6.8$  when  $\kappa/|\Delta'_c| \ll 1$ , such that  $|\Delta'_c| = 9.9|\omega_g|$ . We display the experimental parameters that lead to these rates in the SM [59]. The colored lines represent the PDD model ( $\omega = 2\omega_g$ ). Meanwhile, the black lines are the results of OAT ( $\omega = 0$ ) for  $\kappa/|\Delta'_c| = 10^{-5}$  (solid black line) and  $\kappa/|\Delta'_c| = 10^{-2}$  (dashed black line).

between  $|0\hbar k\rangle \leftrightarrow |2\hbar k\rangle$  while being energetically far from coupling to the  $|-2\hbar k\rangle$  and  $|4\hbar k\rangle$  states, truncating the momentum space to a collective two-level system (see SM [59]). We therefore define the collective momentum operators  $\hat{J}_\pm = \sum_j |2\hbar k\rangle\langle 0\hbar k|_j = \hat{J}_\pm^\dagger$ .

We then displace the cavity field to account for the injected field from the external driving laser [59]. When the injected field is far detuned from the dressed cavity frequency, this displaced cavity field can be adiabatically eliminated with the result [59, 62]

$$\hat{H}_{\text{VC}} = \hbar\omega_g \hat{J}_z - \hbar\chi(t) \hat{J}_x^2, \quad (8)$$

where we have defined the injected light field and the nonlinear interaction rate [59]

$$\beta(t) \approx -\frac{\eta(t)}{\Delta'_c - \frac{i\kappa}{2}}, \quad \chi(t) = \frac{\Delta'_c U_0^2 |\beta|^2}{(\Delta'_c)^2 + \frac{\kappa^2}{4}}. \quad (9)$$

Here,  $\omega_g = 4\omega_r - 2kg\tau$  with recoil frequency  $\omega_r$ ,  $U_0$  is the light-momentum coupling strength [45, 59], and we have defined the dressed pump-cavity detuning  $\Delta'_c$  that includes the Stark shift from the atoms  $\Delta'_c = \Delta_c - NU_0$ . We present a table outlining the various approximations that we assume to be valid to derive Eq. (8) in the SM [59], as well as relevant experimental parameters that satisfy these conditions.

We now wish to reverse engineer the driving profile  $\eta(t)$  such that Eq. (8) simplifies to the PDD Hamiltonian from Eq. (1). For this, we require  $\beta(t) = \beta_0 \sqrt{\cos(\omega t)}$  and so we set  $\eta \propto \sqrt{\cos(\omega t)}$  which amounts to varying the amplitude and phase of the driving laser. However, since

$\chi \propto |\beta|^2$ , this does not yet have the needed harmonics to parametrically drive TACT in Eq. (8). Therefore, we also oscillate the cavity detuning such that  $\Delta'_c(t) = \Delta'_c(0) \text{sgn}[\cos(\omega t)]$ . This promotes  $|\cos(\omega t)| \rightarrow \cos(\omega t)$  whereupon one sets  $\omega = 2\omega_g$ . The oscillation of  $\Delta'_c$  can be accomplished with a time-dependent pump frequency or with time-dependent laser powers when one adds a second pump laser with shifted frequency. With this oscillation, Eq. (8) reduces to the PDD model of Eq. (1),

$$\hat{H}_{\text{VC}} = \hbar\omega_g \hat{J}_z - \hbar\chi_0 \cos(\omega t) \hat{J}_x^2, \quad (10)$$

where  $\chi_0 = U_0^2 |\beta_0|^2 \Delta'_c(0) / [(\Delta'_c(0))^2 + \kappa^2/4]$ .

Since the cavity decays, we also obtain an effective jump operator

$$\hat{L} = \sqrt{\frac{\kappa U_0^2 |\beta_0|^2 |\cos(\omega t)|}{(\Delta'_c)^2 + \frac{\kappa^2}{4}}} \hat{J}_x, \quad (11)$$

from the adiabatic elimination of the cavity (see SM [59]). We can now evolve the system's density matrix  $\hat{\rho}$  under the Born-Markov master equation

$$\frac{\partial \hat{\rho}}{\partial t} = -\frac{i}{\hbar} [\hat{H}_{\text{VC}}(t), \hat{\rho}] + \hat{\mathcal{D}}[\hat{L}(t)]\hat{\rho}, \quad (12)$$

where the Lindbladian superoperator is given by  $\hat{\mathcal{D}}[\hat{O}]\hat{\rho} = \hat{O}\hat{\rho}\hat{O}^\dagger - (\hat{O}^\dagger\hat{O}\hat{\rho} + \hat{\rho}\hat{O}^\dagger\hat{O})/2$ . In Fig. 3(b), we display the results for the maximum QFI, given by Eq. (2), for a density matrix evolved under Eq. (12) with different dissipation rates. For comparison, we also display results for OAT ( $\omega = 0$ ) with  $\kappa/|\Delta'_c| = 10^{-5}$  (solid black line) and  $\kappa/|\Delta'_c| = 10^{-2}$  (dashed black line). Notably, we find that even with a three orders of magnitude larger dissipation rate, the PDD model ( $\omega = 2\omega_g$ ) outperforms OAT on short timescales, which can be seen by comparing the dotted brown line to the solid black line.

To put our results into an experimental context, we adopt the setup of Refs. [44, 45] in which the atoms are allowed to fall for  $\tau = 20$  ms before the pump is turned on. This corresponds to  $|\omega_g| \sim 2\pi \times 0.5$  MHz such that  $|\omega| \sim 2\pi \times 1$  MHz. Therefore, Fig. 3(b) shows an appreciable advantage of the PDD model compared to OAT after  $O(100 \mu\text{s})$ . Furthermore, using the parameters of Fig. 3(b) with small dissipation rates  $\kappa/|\Delta'_c| \ll 1$ , we find  $N\chi_0 \approx 0.012|\omega_g|$  and so Eq. (7) gives  $t_{\text{peak}} \sim 355 \mu\text{s}$  while the OAT plateau time is  $t_{\text{pl}} \sim 1.1$  ms. On the timescale of  $t_{\text{peak}}$ , an effective dephasing effect occurs from the increased energy difference between the momentum states as time progresses, which is accounted for in Ref. [44] by a spin echo sequence [53]. Furthermore, this dephasing is a single particle effect and so increasing  $N$  can grow the collective squeezing rate without increasing the effective dephasing rate. We also confirm that the QCRB is saturated from the simple quadrature measurements considered in the previous section, which can be implemented in the experiment by performing fluorescent measurements

after a Mach–Zehnder interferometry sequence [43]. For the case of  $\kappa \approx |\Delta'_c|/87$ , which corresponds to the cavity decay of Ref. [44], we find that the PDD model reaches a maximum of  $G = 7.5$  dB during the initial squeezing.

*Conclusion and outlook.*— Similar to parametric driving of nonlinear optical interactions to create non-classical states of light [63], in this Letter, we propose an analogous procedure to create non-classical states of matter through parametric driving. While we have focused on long-range interparticle interactions mediated through a dispersive cavity mode, our periodic driving methodology should be more broadly applicable to any system with controllable nonlinearities, such as trapped ions with phonon-mediated interactions [64–68], Bose-Einstein condensates with short- and long-range interactions [69–71], and solid state materials with spin-spin interactions [72–74]. Our periodic driving scheme is distinct from previous modulation proposals [32, 37] as it is implemented by simple parameter modulation of classical driving fields, thereby allowing direct modulation of nonlinear Hamiltonian terms. Unlike previous works on bosonic-mediated quantum amplification [75–77], the protocol presented here does not require squeezed bosonic modes and instead amplifies nonlinearities in the underlying matter to create non-classical, squeezed states. We have demonstrated that our proposed method can potentially be implemented in a current, state-of-the-art VC experiment [43, 44], which would be the first experimental realization of TACT. The system achieves HL scaling in reasonable timescales and has a simple optimal measurement basis, and therefore is a promising platform to create matterwave sensors with a true quantum advantage. Furthermore, it has been shown [34, 35] that TACT creates the Berry-Wiseman phase state, as well as high overlap with other theoretically studied states [51, 78–80]. Therefore, our proposal offers a promising platform to study previous theoretical work in quantum optics [80] and quantum information science [57, 58] in a controllable experimental spin system.

We thank Peter Zoller, Catie LeDesma, and Kendall Mehling for useful discussions. J.T.R., J.D.W, and M.J.H. acknowledge support from NSF PHY 2317149; NSF OMA 2016244; NSF PHY Grant No. 2207963; and NSF 2231377. S.B.J. and S.E. acknowledge support from the Deutsche Forschungsgemeinschaft (DFG): Projects A4 and A5 in SFB/Transregio 185: “OSCAR”.

---

[1] C. Davisson and L. H. Germer, *Nature* **119**, 558 (1927).  
 [2] S. J. Freedman and J. F. Clauser, *Phys. Rev. Lett.* **28**, 938 (1972).  
 [3] G. M. Clemence, *Rev. Mod. Phys.* **19**, 361 (1947).  
 [4] I. I. Shapiro, G. H. Pettengill, M. E. Ash, M. L. Stone, W. B. Smith, R. P. Ingalls, and R. A. Brockelman, *Phys. Rev. Lett.* **20**, 1265 (1968).

[5] B. P. Abbott *et al.* (LIGO Scientific Collaboration and Virgo Collaboration), *Phys. Rev. Lett.* **116**, 061102 (2016).  
 [6] B. P. Abbott *et al.* (LIGO Scientific Collaboration and Virgo Collaboration), *Phys. Rev. X* **6**, 041015 (2016).  
 [7] J. Aasi, J. Abadie, B. Abbott, R. Abbott, T. Abbott, M. Abernathy, C. Adams, T. Adams, P. Addesso, R. Adhikari, *et al.*, *Nature Photonics* **7**, 613 (2013).  
 [8] T. Bothwell, C. J. Kennedy, A. Aeppli, D. Kedar, J. M. Robinson, E. Oelker, A. Staron, and J. Ye, *Nature* **602**, 420 (2022).  
 [9] M. A. Taylor and W. P. Bowen, *Physics Reports* **615**, 1 (2016), quantum metrology and its application in biology.  
 [10] S. Templier, P. Cheiney, Q. d’Armagnac de Castanet, B. Gouraud, H. Porte, F. Napolitano, P. Bouyer, B. Battelier, and B. Barrett, *Science Advances* **8**, eadd3854 (2022).  
 [11] K. Akiyama *et al.* (Event Horizon Telescope Collaboration), *The Astrophysical Journal Letters* **930**, L12 (2022).  
 [12] C. Xue, J.-P. Liu, Q. Li, J.-F. Wu, S.-Q. Yang, Q. Liu, C.-G. Shao, L.-C. Tu, Z.-K. Hu, and J. Luo, *National Science Review* **7**, 1803 (2020).  
 [13] T. S. Roussy, L. Caldwell, T. Wright, W. B. Cairncross, Y. Shagam, K. B. Ng, N. Schlossberger, S. Y. Park, A. Wang, J. Ye, and E. A. Cornell, *Science* **381**, 46 (2023).  
 [14] B. Abi *et al.* (Muon  $g-2$  Collaboration), *Phys. Rev. Lett.* **126**, 141801 (2021).  
 [15] T. Albahri *et al.* (Muon  $g-2$  Collaboration), *Phys. Rev. D* **103**, 072002 (2021).  
 [16] L. Morel, Z. Yao, P. Cladé, and S. Guellati-Khélifa, *Nature* **588**, 61 (2020).  
 [17] G. Agazie *et al.*, *The Astrophysical Journal Letters* **951**, L8 (2023).  
 [18] M. Tse *et al.*, *Phys. Rev. Lett.* **123**, 231107 (2019).  
 [19] E. Pedrozo-Peñafiel, S. Colombo, C. Shu, A. F. Adiyatullin, Z. Li, E. Mendez, B. Braverman, A. Kawasaki, D. Akamatsu, Y. Xiao, and V. Vuletić, *Nature* **588**, 414–418 (2020).  
 [20] O. Hosten, N. J. Engelsen, R. Krishnakumar, and M. A. Kasevich, *Nature* **529**, 505 (2016).  
 [21] J. M. Robinson, M. Miklos, Y. M. Tso, C. J. Kennedy, D. Kedar, J. K. Thompson, and J. Ye, *arXiv preprint arXiv:2211.08621* (2022).  
 [22] B. K. Malia, Y. Wu, J. Martínez-Rincón, and M. A. Kasevich, *Nature* **612**, 661 (2022).  
 [23] R. H. Dicke, *Phys. Rev.* **93**, 99 (1954).  
 [24] K. Hepp and E. H. Lieb, *Annals of Physics* **76**, 360 (1973).  
 [25] K. Baumann, C. Guerlin, F. Brennecke, and T. Esslinger, *Nature* **464**, 1301 (2010).  
 [26] F. Dimer, B. Estienne, A. S. Parkins, and H. J. Carmichael, *Phys. Rev. A* **75**, 013804 (2007).  
 [27] J. T. Reilly, S. B. Jäger, J. Cooper, and M. J. Holland, *Phys. Rev. A* **106**, 023703 (2022).  
 [28] R. Chitra and O. Zilberberg, *Phys. Rev. A* **92**, 023815 (2015).  
 [29] M. Kitagawa and M. Ueda, *Phys. Rev. A* **47**, 5138 (1993).  
 [30] C. K. Law, H. T. Ng, and P. T. Leung, *Phys. Rev. A* **63**, 055601 (2001).  
 [31] A. André and M. D. Lukin, *Phys. Rev. A* **65**, 053819 (2002).  
 [32] W. Huang, Y.-L. Zhang, C.-L. Zou, X.-B. Zou, and G.-C.

- Guo, Phys. Rev. A **91**, 043642 (2015).
- [33] Y. C. Liu, Z. F. Xu, G. R. Jin, and L. You, Phys. Rev. Lett. **107**, 013601 (2011).
- [34] E. Yukawa, G. J. Milburn, C. A. Holmes, M. Ueda, and K. Nemoto, Phys. Rev. A **90**, 062132 (2014).
- [35] D. Kajtoch and E. Witkowska, Phys. Rev. A **92**, 013623 (2015).
- [36] T. b. u. Opatrný, Phys. Rev. A **91**, 053826 (2015).
- [37] L.-N. Wu, M. K. Tey, and L. You, Phys. Rev. A **92**, 063610 (2015).
- [38] I. Kruse, K. Lange, J. Peise, B. Lücke, L. Pezzè, J. Arlt, W. Ertmer, C. Lisdat, L. Santos, A. Smerzi, and C. Klempt, Phys. Rev. Lett. **117**, 143004 (2016).
- [39] J. Borregaard, E. J. Davis, G. S. Bentsen, M. H. Schleier-Smith, and A. S. Sørensen, New Journal of Physics **19**, 093021 (2017).
- [40] F. Anders, L. Pezzè, A. Smerzi, and C. Klempt, Phys. Rev. A **97**, 043813 (2018).
- [41] J. Zhang, S. Wu, Y. Zhang, and Z. Zhou, Science China Information Sciences **64**, 122502 (2021).
- [42] T. Hernández Yanes, M. Plodzień, M. Mackoít Sinkevičienė, G. Žlabys, G. Juzeliūnas, and E. Witkowska, Phys. Rev. Lett. **129**, 090403 (2022).
- [43] G. P. Greve, C. Luo, B. Wu, and J. K. Thompson, Nature **610**, 472 (2022).
- [44] C. Luo, H. Zhang, V. P. Koh, J. D. Wilson, A. Chu, M. J. Holland, A. M. Rey, and J. K. Thompson, arXiv preprint arXiv:2304.01411 (2023).
- [45] J. D. Wilson, C. Luo, J. T. Reilly, H. Zhang, A. Chu, A. M. Rey, M. J. Holland, and J. K. Thompson, Momentum based entanglement in a vertical cavity (2023), (to be published).
- [46] H. Zhang, A. Chu, C. Luo, J. K. Thompson, and A. M. Rey, Phys. Rev. Res. **5**, L032039 (2023).
- [47] J. T. Reilly, J. D. Wilson, S. B. Jäger, C. Wilson, and M. J. Holland, Phys. Rev. Lett. **131**, 150802 (2023).
- [48] L. Pezzè, A. Smerzi, M. K. Oberthaler, R. Schmied, and P. Treutlein, Rev. Mod. Phys. **90**, 035005 (2018).
- [49] P. Kirton, M. M. Roses, J. Keeling, and E. G. Dalla Torre, Advanced Quantum Technologies **2**, 1800043 (2019).
- [50] J. Liu, H. Yuan, X.-M. Lu, and X. Wang, Journal of Physics A: Mathematical and Theoretical **53**, 023001 (2019).
- [51] M. J. Holland and K. Burnett, Phys. Rev. Lett. **71**, 1355 (1993).
- [52] M. Xu, D. A. Tieri, and M. J. Holland, Phys. Rev. A **87**, 062101 (2013).
- [53] D. A. Steck, Quantum and atom optics (2007).
- [54] C. M. Caves, Advanced Quantum Technologies **3**, 1900138 (2020).
- [55] T. Holstein and H. Primakoff, Phys. Rev. **58**, 1098 (1940).
- [56] T. Byrnes and E. O. Ilo-Okeke, *Quantum atom optics: Theory and applications to quantum technology* (Cambridge university press, 2021).
- [57] D. W. Berry, *Adaptive Phase Measurements*, Ph.D. thesis, University of Queensland, Queensland (2001).
- [58] D. W. Berry, B. L. Higgins, S. D. Bartlett, M. W. Mitchell, G. J. Pryde, and H. M. Wiseman, Phys. Rev. A **80**, 052114 (2009).
- [59] See Supplemental Material which includes Ref. [81–85]. Here, we comment on the states created by the PDD model, display a full derivation of achieving the PDD in the vertical cavity experiment, and comment on relevant experimental parameters that satisfy the needed approximations to achieve the PDD model.
- [60] J. T. Reilly, *Entropy Removal and Coherence with Lasers*, Bachelor's thesis, University of Colorado Boulder (2020).
- [61] L. Pezzè and A. Smerzi, Phys. Rev. Lett. **102**, 100401 (2009).
- [62] S. B. Jäger, T. Schmit, G. Morigi, M. J. Holland, and R. Betzholz, Phys. Rev. Lett. **129**, 063601 (2022).
- [63] T. J. Kippenberg, S. M. Spillane, and K. J. Vahala, Phys. Rev. Lett. **93**, 083904 (2004).
- [64] J. D. Sterk, L. Luo, T. A. Manning, P. Maunz, and C. Monroe, Phys. Rev. A **85**, 062308 (2012).
- [65] R. B. Linnet, I. D. Leroux, M. Marciante, A. Dantan, and M. Drewsen, Phys. Rev. Lett. **109**, 233005 (2012).
- [66] A. C. Wilson, Y. Colombe, K. R. Brown, E. Knill, D. Leibfried, and D. J. Wineland, Nature **512**, 57 (2014).
- [67] J. G. Bohnet, B. C. Sawyer, J. W. Britton, M. L. Wall, A. M. Rey, M. Foss-Feig, and J. J. Bollinger, Science **352**, 1297 (2016).
- [68] A. Kahan, L. Ermann, and C. Cormick, Phys. Rev. A **104**, 043705 (2021).
- [69] A. N. Pyrkov and T. Byrnes, New Journal of Physics **15**, 093019 (2013).
- [70] R. M. Kroeze, Y. Guo, V. D. Vaidya, J. Keeling, and B. L. Lev, Phys. Rev. Lett. **121**, 163601 (2018).
- [71] F. Mivehvar, H. Ritsch, and F. Piazza, Phys. Rev. Lett. **122**, 113603 (2019).
- [72] H. Zhou, J. Choi, S. Choi, R. Landig, A. M. Douglas, J. Isoya, F. Jelezko, S. Onoda, H. Sumiya, P. Cappellaro, H. S. Knowles, H. Park, and M. D. Lukin, Phys. Rev. X **10**, 031003 (2020).
- [73] T. Xie, Z. Zhao, X. Kong, W. Ma, M. Wang, X. Ye, P. Yu, Z. Yang, S. Xu, P. Wang, Y. Wang, F. Shi, and J. Du, Science Advances **7**, eabg9204 (2021).
- [74] J. Lee, M. Tatsuta, A. Xu, E. Bauch, M. J. H. Ku, and R. L. Walsworth, NPJ Quantum Information **9**, 77 (2023).
- [75] X.-Y. Lü, Y. Wu, J. R. Johansson, H. Jing, J. Zhang, and F. Nori, Phys. Rev. Lett. **114**, 093602 (2015).
- [76] S. Zeytinoglu, A. m. c. İmamoğlu, and S. Huber, Phys. Rev. X **7**, 021041 (2017).
- [77] S. C. Burd, R. Srinivas, H. M. Knaack, W. Ge, A. C. Wilson, D. J. Wineland, D. Leibfried, J. J. Bollinger, D. T. C. Allcock, and D. H. Slichter, Nature Physics **17**, 898 (2021).
- [78] B. Yurke and D. Stoler, Phys. Rev. Lett. **57**, 13 (1986).
- [79] J. K. Stockton, J. M. Geremia, A. C. Doherty, and H. Mabuchi, Phys. Rev. A **67**, 022112 (2003).
- [80] J. Combes and H. M. Wiseman, Journal of Optics B: Quantum and Semiclassical Optics **7**, 14 (2004).
- [81] A. S. Holevo, in *Quantum Probability and Applications to the Quantum Theory of Irreversible Processes*, edited by L. Accardi, A. Frigerio, and V. Gorini (Springer Berlin Heidelberg, Berlin, Heidelberg, 1984) pp. 153–172.
- [82] L. Susskind and J. Glogower, Physics Physique Fizika **1**, 49 (1964).
- [83] I. Gradshteyn and I. Ryzhik, *Table of Integrals, Series, and Products*, 6th ed., edited by D. Zwillinger and A. Jeffrey (Elsevier Science, 2000).
- [84] A. Metelmann, O. Lanes, T. Chien, A. McDonald, M. Hatridge, and A. Clerk, arXiv preprint arXiv:2208.00024 (2022).

[85] D. A. Steck, Rubidium 87 d line data (2001).

# Supplemental Material: Speeding Up Squeezing with a Periodically Driven Dicke Model

Jarrod T. Reilly,<sup>1</sup> Simon B. Jäger,<sup>2</sup> John Drew Wilson,<sup>1</sup> John Cooper,<sup>1</sup> Sebastian Eggert,<sup>2</sup> and Murray J. Holland<sup>1</sup>

<sup>1</sup>*JILA, NIST, and Department of Physics, University of Colorado, 440 UCB, Boulder, CO 80309, USA*

<sup>2</sup>*Physics Department and Research Center OPTIMAS,*

*University of Kaiserslautern-Landau, D-67663, Kaiserslautern, Germany*

(Dated: October 12, 2023)

## CONTENTS

I. States Created by the Periodically Driven Dicke Model	1
A. Berry-Wiseman Phase State	1
B. State with Peak QFI	1
II. Model for Periodically Driving a Vertical Cavity	2
A. Starting Point	3
B. Elimination of the Electronic Excited State	3
C. Displacement of the Cavity Field	3
D. Adiabatic Elimination of the Cavity Field	4
E. Reduction to Two Momentum States	5
III. Profile of the Injected Field	6
IV. Experimental Parameters	7
References	7

## I. STATES CREATED BY THE PERIODICALLY DRIVEN DICKE MODEL

In this section, we comment on some of the properties of two states that the periodically driven Dicke (PDD) model creates. We focus on the states examined in Fig. 2 of the Main Text, namely, the Berry-Wiseman (BW) phase state  $\hat{\rho}_{\text{BW}}$  and the state with the peak QFI  $\hat{\rho}_{\text{peak}}$ .

### A. Berry-Wiseman Phase State

We begin by discussing the BW phase state, whose Q-function is shown in Fig 1(b) of the Main Text. The Holevo variance for an ensemble of pseudospin-1/2 particles is defined as [1, 2]

$$V(\varphi)_\psi \equiv |\langle e^{-i\varphi} \rangle_\psi|^2 - 1, \quad (\text{S1})$$

where

$$\begin{aligned} \langle e^{-i\varphi} \rangle_\psi &\equiv \int_0^{2\pi} P_\psi(\varphi) e^{-i\varphi} d\varphi, \\ P_\psi(\varphi) &\equiv \langle \psi | e^{-i\varphi \hat{J}_z} | \psi \rangle. \end{aligned} \quad (\text{S2})$$

This variance is useful because states with complete phase uncertainty (e.g., any  $|\psi\rangle = |j = N/2, m\rangle$ ) will

have infinite Holevo variance, whereas the typical phase variance [2],  $\Delta\varphi^2 = \langle \varphi^2 \rangle_\psi - \langle \varphi \rangle_\psi^2$ , has a maximum uncertainty of  $\Delta\varphi = 2\pi$ . It has been shown [2, 3] that the state which minimizes the Holevo variance is the BW phase state,

$$|\psi_{\text{BW}}\rangle = \frac{1}{\sqrt{\frac{N}{2} + 1}} \sum_{m=-\frac{N}{2}}^{\frac{N}{2}} \sin\left[\frac{\pi(\frac{N}{2} + m + 1)}{N + 2}\right] \left| \frac{N}{2}, m \right\rangle, \quad (\text{S3})$$

such that  $\hat{\rho}_{\text{BW}} = |\psi_{\text{BW}}\rangle\langle\psi_{\text{BW}}|$ . This state has  $V(\varphi)_{\text{BW}} = \pi^2/N^2$  and is notably an eigenstate of the Susskind cosine operator [4],

$$\widehat{\text{cos}}(\varphi) \equiv \frac{1}{2} \sum_{m=-N/2}^{N/2} \left( \left| \frac{N}{2}, m + 1 \right\rangle \left\langle \frac{N}{2}, m \right| + \text{H.c.} \right). \quad (\text{S4})$$

The BW phase state is of particular interest for phase estimation because its dynamic range is a full  $2\pi$ , meaning  $\langle \psi_{\text{BW}} | e^{-i\varphi \hat{J}_z} | \psi_{\text{BW}} \rangle = 1$  only if  $\varphi = n2\pi$  for integer  $n$ . Simultaneously, it has a quantum Fisher information (QFI) reaching Heisenberg limit (HL) scaling at

$$\mathcal{F}_{\text{BW}} \approx \left( \frac{1}{3} - \frac{2}{\pi^2} \right) N^2 \approx 0.13N^2. \quad (\text{S5})$$

These conditions guarantee that, with no a priori knowledge of  $\varphi$ , the BW phase state is the optimal state to gain information in a single measurement [5], making it a useful state for a multitude of sensing applications. For example, creating a BW phase state in matterwave interferometry would guarantee that each measurement gives the highest resolution estimation of an acceleration, which would be a powerful tool for time-varying gravitational fields such as those that an orbiting satellite experiences.

### B. State with Peak QFI

We now discuss the state with the maximum QFI during the initial squeezing under the PDD model,  $\hat{\rho}_{\text{peak}}$ . We display the Q-function of this state in Fig. 1(a) which shows that  $\hat{\rho}_{\text{peak}}$  has properties of a partial ring state [6]. One would expect this structure to be highly sensitive to rotations about  $\hat{J}_z$  and a point on the Bloch sphere's equator in the direction of the anti-squeezed

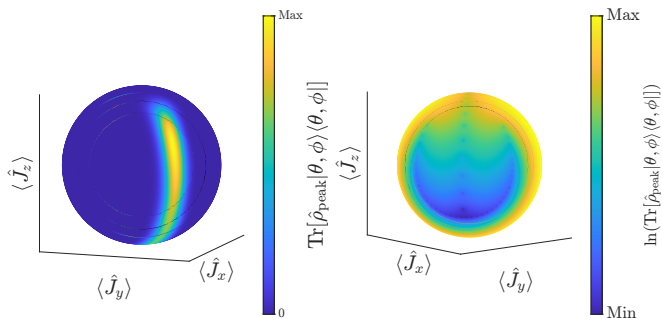


FIG. 1. The state with the maximum QFI  $\hat{\rho}_{\text{peak}}$  for  $N = 100$ . (a) The Q-function calculated by finding the overlap with the coherent spin state  $|\theta, \phi\rangle$  at every point on the Bloch sphere. (b) The log of the Q-function to make the interference fringes more pronounced.

axis. This explains why the two largest eigenvalues of the QFIM in Fig. 2(a) of the Main Text correspond to  $\hat{G} = (\hat{J}_x + \hat{J}_y)/\sqrt{2}$  and  $\hat{G}_2 = \hat{J}_z$  in the rotating frame. Moreover, by taking a log of the Q-function, which we show in Fig. 1(b), one can see interference fringes form around part of a longitude line of the Bloch sphere. This is reminiscent of the interference fringes that are present in the  $N00N$  state [3, 7] and may explain why the state is more sensitive to rotations about  $\hat{G}$  than  $\hat{J}_z$ .

As the squeezing continues past  $\hat{\rho}_{\text{peak}}$  under the PDD model with small dissipation, the large population packets begin to converge towards each other at the north pole. However, the state's QFI remains larger than the SQL as interference fringes remain present with a small amount of population still in a partial ring. The state reaches a local minimum in QFI when the large population packets meet at the north pole, but then the QFI climbs back to  $\lambda_{\text{max}} > N^2/2$  as a ring-like structure reemerges. This ring-like state has  $\hat{G} = \hat{J}_z$ .

We can also briefly comment on the case of non-negligible dissipation. Damping of the fringes shown in Fig. 1(b) may explain why the optimal generator switches from  $\hat{G}$  to  $\hat{J}_z$  in the double peak structure of Fig. 3(b) of the Main Text when  $\kappa/|\Delta'_c| \gtrsim 10^{-2}$ . Here, the first peak corresponds to the initial squeezing with  $\hat{G} = (\hat{J}_x + \hat{J}_y)/\sqrt{2}$ , but now with a lower QFI that reaches its maximum value more quickly. The optimal generator then switches to  $\hat{J}_z$  for the second peak as the QFI with respect to  $\hat{J}_z$  rotations falls off less quickly when increas-

ing  $\kappa$ .

## II. MODEL FOR PERIODICALLY DRIVING A VERTICAL CAVITY

This section is dedicated to deriving the effective model for the vertical cavity (VC) experiment. We further discuss how the periodically driven Dicke model can be implemented in this system. We consider the experimental VC setup displayed schematically in Fig. 3(a) of the Main

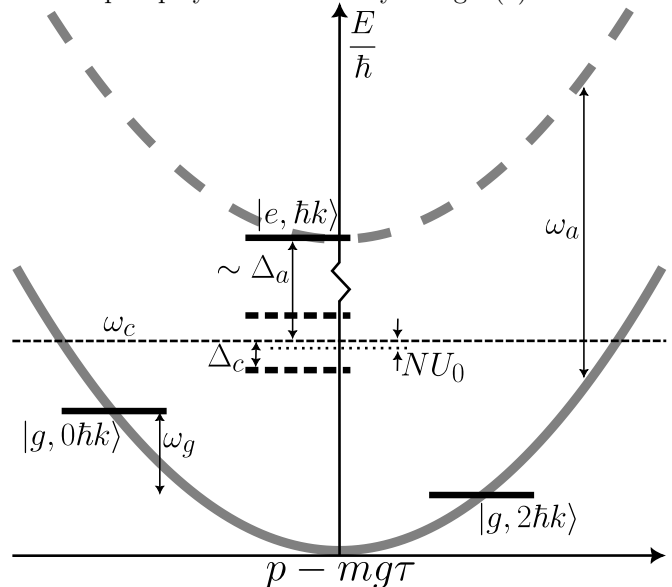


FIG. 2. Schematic diagram of the frequency spectrum of a single atom in the vertical cavity setup. The states are labeled by their initial momentum value, i.e.,  $|i, p_0 - mg\tau\rangle \rightarrow |i, p_0\rangle$ .

Text. We also show an energy diagram of each atom in the system after they have fallen for a certain time  $\tau$  in Fig. 2. The internal states  $|g\rangle \equiv |F = 2, m_F = 2\rangle$  and  $|e\rangle \equiv |F' = 3, m_{F'} = 3\rangle$  are separated by an optical frequency  $\omega_a$  and we assume a closed-cycling transition where  $|g\rangle$  can decay back to  $|e\rangle$  at a rate  $\gamma$ . The atoms interact with a single mode of an optical cavity, which has frequency  $\omega_c$ , at a single atom vacuum coupling rate  $\Lambda$ . A coherent field is injected into the cavity which drives the mode with a time-dependent rate  $|\eta(t)|$  and frequency  $\omega_p(t)$ . The modulation of the frequency  $\omega_p(t) = \omega_p^{(0)} + \omega_p^{(1)}(t)$  is chosen to be around a frequency  $\omega_p^{(0)}$  with a fixed detuning to the atoms  $\Delta_a = \omega_a - \omega_p^{(0)}$  and the cavity  $\Delta_c = \omega_c - \omega_p^{(0)}$ .

### A. Starting Point

Our theoretical analysis starts with the master equation for the density matrix  $\hat{\rho}_{\text{apc}}$  describing the atomic internal and motional degrees of freedom, as well as the cavity degree of freedom. The master equation is given by

$$\frac{\partial \hat{\rho}_{\text{apc}}}{\partial t} = -\frac{i}{\hbar} \left[ \hat{H}_{\text{apc}}, \hat{\rho}_{\text{apc}} \right] + \hat{\mathcal{D}} \left[ \sqrt{\kappa} \hat{a} \right] \hat{\rho}_{\text{apc}} + \sum_j \hat{\mathcal{D}} \left[ \sqrt{\gamma} \hat{\sigma}_j^- \right] \hat{\rho}_{\text{apc}}, \quad (\text{S6})$$

where the coherent dynamics are governed by the Hamiltonian

$$\hat{H}_{\text{apc}} = \sum_j \left[ \frac{(\hat{p}_j - mg\tau)^2}{2m} + \hbar \Lambda \cos(k\hat{x}_j) (\hat{a}^\dagger \hat{\sigma}_j^- + \hat{\sigma}_j^+ \hat{a}) + \hbar \Delta_a \hat{\sigma}_j^+ \hat{\sigma}_j^- \right] + \hbar \Delta_c \hat{a}^\dagger \hat{a} + \hbar [\eta(t) \hat{a}^\dagger + \text{H.c.}]. \quad (\text{S7})$$

The first term in the Hamiltonian describes the kinetic energy with momentum operators  $\hat{p}_j$  of the atoms with mass  $m$  after falling for a time  $\tau$  under acceleration  $g$ . The second term corresponds to the atomic-cavity coupling, where  $\cos(kx)$  is the standing-wave mode function of the cavity evaluated at the atomic position operators  $\hat{x}_j$  with wavenumber  $k$ . In addition, we have introduced the creation and annihilation operators  $\hat{a}^\dagger$  and  $\hat{a}$  for the cavity mode and the internal excitation  $\hat{\sigma}_j^+ = |e\rangle_j \langle g|_j$  and  $\hat{\sigma}_j^- = |g\rangle_j \langle e|_j$ , respectively. The third term in Eq. (S7) is the energy of the excited state in the frame rotating with  $\omega_p^{(0)}$ . The last two terms describe the energy of the photons and the driving of the cavity mode where modulations of frequency  $\omega_p^{(1)}(t)$  and amplitude  $|\eta(t)|$  are encoded in the complex and time-dependent frequency  $\eta(t)$ . In addition to the coherent effects, the master equation also includes cavity photon losses with rate  $\kappa$  and spontaneous emission with rate  $\gamma$ . The Lindblad superoperator  $\hat{\mathcal{D}}$  for these Markov processes is defined as

$$\hat{\mathcal{D}}[\hat{O}]\hat{\rho} = -\frac{1}{2}[\hat{O}^\dagger \hat{O} \hat{\rho} + \hat{\rho} \hat{O}^\dagger \hat{O} - 2\hat{O} \hat{\rho} \hat{O}^\dagger]. \quad (\text{S8})$$

### B. Elimination of the Electronic Excited State

We work in the regime where the detuning  $|\Delta_a|$  is much larger than the spontaneous emission rate and any characteristic frequency determining the dynamics of the cavity and the atomic external degrees of freedom. In this regime, the atoms remain, to good approximation, in the electronic ground state and the dominant scattering process is coherent scattering of laser photons. In addition, we assume that the fixed atom-laser detuning is much larger than the dynamical variance of the frequency  $|\Delta_a| \gg \omega_p^{(1)}$ , which implies that the small modifications in the laser frequency have only a minor effect onto the coherent scattering rates. Using these approximations based on the parameter regime of interest, we derive an effective master equation which governs the dynamics of the density matrix  $\hat{\rho}_{\text{pc}}$  of atomic external degrees of freedom and the cavity. This master equation is given by

$$\frac{\partial \hat{\rho}_{\text{pc}}}{\partial t} = -\frac{i}{\hbar} \left[ \hat{H}_{\text{pc}}, \hat{\rho} \right] + \hat{\mathcal{D}} \left[ \sqrt{\kappa} \hat{a} \right] \hat{\rho}_{\text{pc}}, \quad (\text{S9})$$

with the Hamiltonian [8]

$$\hat{H}_{\text{pc}} = \sum_j \frac{(\hat{p}_j - mg\tau)^2}{2m} + \hbar \Delta'_c \left[ 1 - \frac{U_0}{\Delta'_c} \sum_j \cos(2k\hat{x}_j) \right] \hat{a}^\dagger \hat{a} + \hbar [\eta(t) \hat{a}^\dagger + \text{H.c.}]. \quad (\text{S10})$$

The second term in Eq. (S10) describes the modified frequency of cavity photons which is shifted due to the presence of the atoms. Here,  $\Delta'_c = \Delta_c - NU_0$  is the dressed cavity detuning with the ac Stark shift

$$U_0 = \frac{\Lambda^2 \Delta_a / 2}{\Delta_a^2 + \gamma^2 / 4}. \quad (\text{S11})$$

### C. Displacement of the Cavity Field

Next, we displace the cavity field by the field which is injected by the external laser. This is formally done by applying the displacement transformation

$$\hat{D}_1 = \exp[\hat{a}^\dagger \beta(t) - \beta^*(t) \hat{a}], \quad (\text{S12})$$

onto the density matrix  $\tilde{\rho}_{\text{pc}} = \hat{D}_1^\dagger \hat{\rho}_{\text{pc}} \hat{D}_1$ . In this new displaced picture, we find

$$\frac{\partial \tilde{\rho}_{\text{pc}}}{\partial t} = -\frac{i}{\hbar} [\tilde{\hat{H}}, \tilde{\rho}_{\text{pc}}] + \hat{\mathcal{D}} [\sqrt{\kappa} \hat{a}] \tilde{\rho}_{\text{pc}}, \quad (\text{S13})$$

where the injected light field  $\beta$  follows the differential equation

$$\frac{\partial \beta}{\partial t} = -i \left( \Delta'_c - \frac{i\kappa}{2} \right) \beta - i\eta. \quad (\text{S14})$$

With a solution for this differential equation, we obtain the following displaced Hamiltonian:

$$\tilde{\hat{H}}_{\text{pc}} = \sum_j \left[ \frac{(\hat{p}_j - mg\tau)^2}{2m} - \hbar U_0 \cos(2k\hat{x}_j) (\hat{a}^\dagger \beta + \beta^* \hat{a}) - \hbar U_0 |\beta|^2 \cos(2k\hat{x}_j) \right] + \hbar \Delta'_c \left[ 1 - \epsilon \sum_j \cos(2k\hat{x}_j) \right] \hat{a}^\dagger \hat{a}, \quad (\text{S15})$$

where  $\epsilon = U_0/\Delta'_c$ . We remark that in this displaced picture, there is no external driving of the cavity. Instead, the meaning of  $\hat{a}$  is now the scattered field due to the presence of atoms which, in the original picture, needs to be added to the injected field  $\beta$ .

#### D. Adiabatic Elimination of the Cavity Field

By assuming  $|\Delta'_c|$  is now the largest frequency in the effective system, we are able to adiabatically eliminate the scattered cavity field. This requires that  $|\Delta'_c|$  is much larger than the Doppler-shift of the atoms and also that the modulation of the drive is slow compared to  $1/|\Delta'_c|$ . In this limit, we can derive an effective master equation for the density matrix describing the atomic external degrees of freedom  $\hat{\rho}_{\text{p}}$  [9].

To eliminate the field, we assume that the scattered field is, to a good approximation, in vacuum. We can then displace the field by

$$\hat{D}_2 = \exp[\hat{a}^\dagger \hat{\alpha} - \hat{\alpha}^\dagger \hat{a}], \quad (\text{S16})$$

such that the equation of motion for  $\hat{\rho}$ , where we dropped the ‘‘p’’ index for brevity, is given by [9]

$$\frac{\partial \hat{\rho}}{\partial t} = -\frac{i}{\hbar} [\hat{H}_{\text{VC}}, \hat{\rho}] + \hat{\mathcal{D}} [\sqrt{\kappa} \hat{\alpha}] \hat{\rho}, \quad (\text{S17})$$

with the Hamiltonian

$$\hat{H}_{\text{VC}} = \sum_j \left[ \frac{(\hat{p}_j - mg\tau)^2}{2m} - \hbar U_0 |\beta|^2 \cos(2k\hat{x}_j) \right] - \frac{\hbar U_0}{2} \left[ \beta \hat{\alpha}^\dagger \sum_j \cos(2k\hat{x}_j) + \text{H.c.} \right]. \quad (\text{S18})$$

We then solve for the effective field operator

$$\frac{\partial \hat{\alpha}}{\partial t} = -i \left[ \frac{(\hat{p}_j - mg\tau)^2}{2m}, \hat{\alpha} \right] - i \left[ \Delta'_c \left( 1 - \epsilon \sum_j \cos(2k\hat{x}_j) \right) - \frac{i\kappa}{2} \right] \hat{\alpha} + iU_0 \beta \sum_j \cos(2k\hat{x}_j). \quad (\text{S19})$$

Here, we have assumed that  $U_0|\beta|^2$  is much smaller than any momentum energy gaps (see Section II E for the relevant gaps) such that it can be dropped from the commutator in Eq. (S19).

We are considering parameters such that  $N|\epsilon|/2 \ll 1$  so that we can drop the non-linearity  $\propto \epsilon$  in Eq. (S19). By further making the ansatz  $\hat{\alpha}(t) = a_+(t) \sum_j \exp[2ik\hat{x}_j] + a_-(t) \sum_j \exp[-2ik\hat{x}_j]$ , we can find equations of motion for the coefficients  $a_\pm$ . In the parameter regime  $|\Delta'_c - i\kappa/2| \gg \omega$ , where  $\omega$  is the characteristic modulation frequency of  $\beta$  [see Eqs. (S26) and (S27)], we can integrate the differential equations for  $a_\pm$ . Using the obtained results in  $\hat{\alpha}(t)$  leads to the effective field operator

$$\hat{\alpha}(t) \approx \frac{U_0 \beta}{2} \sum_j \left[ \frac{1}{\Delta'_c + \Delta p_{\pm 2} - \frac{i\kappa}{2}} e^{2ik\hat{x}_j} + \frac{1}{\Delta'_c - \Delta p_{\pm 2} - \frac{i\kappa}{2}} e^{-2ik\hat{x}_j} \right], \quad (\text{S20})$$

where  $\Delta p_{\pm 2} = (p \pm 2\hbar k - mg\tau)^2/(2\hbar m) - (p - mg\tau)^2/(2\hbar m)$ .

We now assume that we are restricted to low energy motional states, which we will formally justify in Sec. II E. For these states, we can set  $\Delta'_c \pm \Delta p_{\pm 2} \approx \Delta'_c$  such that the effective field operator becomes

$$\hat{\alpha}(t) \approx \frac{U_0\beta}{\Delta'_c - \frac{i\kappa}{2}} \sum_j \cos(2k\hat{x}_j). \quad (\text{S21})$$

This is valid if  $\Delta'_c \gg \Delta p_{\pm 2}$  and, for the situation considered here, amounts to  $\Delta'_c \pm \omega_g \approx \Delta'_c$  where  $\omega_g$  is given by Eq. (S27) in Sec. II E.

Using Eq. (S21) in Eqs. (S17) and (S18), we find

$$\frac{\partial \hat{\rho}}{\partial t} \approx -\frac{i}{\hbar} [\hat{H}_{\text{VC}}, \hat{\rho}] + \hat{\mathcal{D}} \left[ \sqrt{\Gamma_c(t)} \sum_j \cos(2k\hat{x}_j) \right] \hat{\rho}, \quad (\text{S22})$$

and the Hamiltonian

$$\hat{H}_{\text{VC}} \approx \sum_j \left[ \frac{(\hat{p}_j - mg\tau)^2}{2m} - \hbar U_0 |\beta|^2 \cos(2k\hat{x}_j) \right] - \hbar \chi(t) \sum_{i,j} \cos(2k\hat{x}_i) \cos(2k\hat{x}_j). \quad (\text{S23})$$

Here, we have defined the nonlinear interaction rate

$$\chi(t) = \frac{\Delta'_c U_0^2 |\beta|^2}{(\Delta'_c)^2 + \kappa^2/4}, \quad (\text{S24})$$

and the dissipation rate

$$\Gamma_c(t) = \frac{\kappa U_0^2 |\beta|^2}{(\Delta'_c)^2 + \kappa^2/4}. \quad (\text{S25})$$

### E. Reduction to Two Momentum States

In our protocol, the atoms are initialized with momentum  $p = 0$ , which means they have the kinetic energy  $Nmg^2\tau^2/2$  after gravitational acceleration. The idea of the periodic driving with  $\eta$  is now to engineer an injected light field  $\beta$  which drives a pair creation process by flipping two momentum state to  $p = 2\hbar k$ . This requires that we must drive with a frequency

$$\omega = 2\omega_g, \quad (\text{S26})$$

where  $\omega_g$  denotes the energy to excite a single atom from  $p = 0\hbar k$  to the momentum state  $p = 2\hbar k$ ,

$$\omega_g = \frac{(2\hbar k - mg\tau)^2 - (mg\tau)^2}{2\hbar m} = 4\omega_r - 2kg\tau. \quad (\text{S27})$$

Here, we have introduced the recoil frequency  $\omega_r = \hbar k^2/(2m)$ . Thus, an appropriate driving profile would realize  $\chi(t) \propto \cos(\omega t)$ . Using Eq. (S24), this can be realized with a driving resulting in  $|\beta(t)|^2 \propto |\cos(\omega t)|$  and  $\Delta'_c \propto \text{sgn}[\cos(\omega t)]$ , as explained in the Main Text. The latter corresponds to switching the driving frequency of the laser with respect to the cavity from red to blue detuned and back periodically in time.

We now want to restrict the dynamics of the atomic motional states to the momentum states  $|p = 0\rangle$  and  $|p = 2\hbar k\rangle$ . This requires that we do not excite other momentum states, which can be justified using time-dependent perturbation theory. The two most relevant momentum flips occur due to (a) the single-particle term proportional to  $\cos(2k\hat{x}_j)$  in Eq. (S23) which induces the momentum flip of a single atom  $p = \pm 2\hbar k$ , and (b) the two-particle term proportional to  $\cos(2k\hat{x}_i) \cos(2k\hat{x}_j)$  in Eq. (S23) which can also amplify a pair with  $p_1 = \pm 2\hbar k$  and  $p_2 = -2\hbar k$ . We examine the requirements to avoid these two processes individually:

(a) The frequency gap for a single flip into the state  $p = \pm 2\hbar k$  is  $\Delta\omega_{\pm}^{(1)}$ . It can be calculated as

$$\Delta\omega_{\pm}^{(1)} = \frac{(\pm 2\hbar k - mg\tau)^2 - (mg\tau)^2}{2m} = 4\omega_r \mp 2kg\tau. \quad (\text{S28})$$

The driving field  $|\beta|^2 \propto |\cos(\omega t)|$  has frequency components that are multiples of  $2\omega = 4\omega_g$ . To neglect single momentum flips, we therefore require

$$\left| \frac{U_0 |\beta|^2}{|4\omega_g - |4\omega_r \mp 2kg\tau|} \right| \ll 1. \quad (\text{S29})$$

For large  $kg\tau \gg 2\omega_r$ , this is true when  $|U_0| |\beta|^2 \ll 6kg\tau$ .

(b) We now determine the frequency gap  $\Delta\omega_{\pm}^{(2)}$  for the unwanted pair creation processes corresponding to creating  $p_1 = \pm 2\hbar k$  and  $p_2 = -2\hbar k$ . The frequency gap is given by

$$\begin{aligned} \Delta\omega_+^{(2)} &= \frac{(2\hbar k - mg\tau)^2 - (mg\tau)^2}{2m} + \frac{(-2\hbar k - mg\tau)^2 - (mg\tau)^2}{2m} = 8\omega_r, \\ \Delta\omega_-^{(2)} &= 2 \frac{(-2\hbar k - mg\tau)^2 - (mg\tau)^2}{2m} = 8\omega_r + 4kg\tau. \end{aligned} \quad (\text{S30})$$

Since we assume  $\chi(t) \propto \cos(\omega t)$  with  $\omega = 2\omega_g$ , these pair creation processes can be neglected if

$$\left| \frac{N\chi}{|2\omega_g - |\Delta\omega_+^{(2)}|} \right| \ll 1. \quad (\text{S31})$$

Again assuming  $kg\tau \gg 2\omega_r$ , this approximation is valid if  $N\chi \ll 16\omega_r$ . In this calculation, we have included a factor of  $N$  because of the collective enhancement.

In the parameter regime where we can reduce the dynamics to atoms with momenta  $p = 0$  and  $p = 2\hbar k$ , we can identify the momentum raising operator as an effective collective spin raising operator

$$\sum_j \exp[2ik\hat{x}_j] \rightarrow \hat{J}_+ = \sum_j |2\hbar k\rangle_j \langle 0\hbar k|_j. \quad (\text{S32})$$

We also define  $\hat{J}_- = \hat{J}_+^\dagger$  as well as the SU(2) basis operators  $\hat{J}_x = (\hat{J}_+ + \hat{J}_-)/2$ ,  $\hat{J}_y = i(\hat{J}_- - \hat{J}_+)/2$ , and  $\hat{J}_z = [\hat{J}_+, \hat{J}_-]/2$ , where we note  $\sum_j \cos(2k\hat{x}_j) \rightarrow \hat{J}_x$ . With these definitions, we can rewrite the Hamiltonian in Eq. (S23) as the periodically driven Dicke (PDD) model

$$\begin{aligned} \hat{H}_{\text{VC}} &= \hbar\omega_g \hat{J}_z - \hbar\chi(t) \hat{J}_x^2 \\ &= \hbar\omega_g \hat{J}_z - \hbar\chi_0 \cos(t) \hat{J}_x^2, \end{aligned} \quad (\text{S33})$$

with  $\chi_0 = U_0^2 |\beta_0|^2 \Delta'_c(0) / ([\Delta'_c(0)]^2 + \kappa^2/4)$ . We also find a dissipative term with jump operator

$$\hat{L} = \sqrt{\Gamma_c(t)} \hat{J}_x, \quad (\text{S34})$$

with  $\Gamma_c(t) \propto |\cos(\omega t)|$ .

### III. PROFILE OF THE INJECTED FIELD

We now comment on the driving profile of the injected field into the VC setup that reproduces the behavior of the periodically driven Dicke model. We begin with the relationship between the injected field and standing field, Eq. (S14). Formally integrating and making a coarse-

graining approximation, we find

$$\begin{aligned} \beta(t) &= e^{-i(\Delta'_c - \frac{i\kappa}{2})t} \beta(0) - i \int_0^t ds e^{-i(\Delta'_c - \frac{i\kappa}{2})s} \eta(t-s) \\ &\approx -\frac{\eta(t)}{\Delta'_c - \frac{i\kappa}{2}}, \end{aligned} \quad (\text{S35})$$

where we have assumed that the temporal variation of  $\eta$  is slow compared to the exponential kernel in the integral. Within this limit, we can now reverse engineer  $\eta(t)$  by simply inverting Eq. (S35).

In the case that the coarse-graining approximation used in Eq. (S35) breaks down, one can instead plug

$\beta(t) = \beta_0 \sqrt{\cos(\omega t)}$  into Eq. (S14) with the result

$$\eta(t) = -\frac{i\omega\beta_0}{2} \sqrt{\sin(\omega t) \tan(\omega t)} - \beta_0 \left( \Delta'_c - \frac{i\kappa}{2} \right) \sqrt{\cos(\omega t)}. \quad (\text{S36})$$

While the second term in this equation is the adiabatic result of the driving profile, the first term exhibits divergences which originate from the non-analyticities of  $\sqrt{\tan(\omega t)}$ . The first term contributes a factor of  $\sqrt{\omega/\Delta'_c}$  in the integral for  $\beta(t)$ , Eq. (S35). In an integral over  $\beta(t)$ , it will be suppressed by a factor of  $(\omega/\Delta'_c)^{3/2}$  [10], and so the second term in Eq. (S36) will be the dominate contribution. However, for experimental considerations, it might be advantageous to use a profile with smooth intensity profile. In general, it might be interesting to explore several other driving profiles such as  $\eta(t) \propto \text{sgn}[\cos(\omega t)]$  (square wave) and  $\eta(t) \propto 1 - 2 \arccos[\cos(\omega t)]/\pi$  (triangle wave). We expect that these profiles can have similar performances for squeezing although they might lead to shifted parametric resonances for  $\omega$  [11] which can be derived using a Holstein-Primakoff approximation [12, 13] for early times. For practical applications, it is also of interest to optimize  $\eta(t)$  in order to achieve the maximum squeezing in minimum time with given experimental constraints. These considerations are left for future work.

#### IV. EXPERIMENTAL PARAMETERS

In this section, we present experimental parameters that lead to the values of  $\omega_g$ ,  $\beta_0$ ,  $U_0$ , and  $\Delta'_c$  used in Fig. 3(b) of the Main Text. We use  $N = 100$  throughout this section. We then begin with the single-atom coupling constant of the cavity used in Ref. [14],  $\Lambda = 2\pi \times 0.5$  MHz. For this section, we also use the cavity loss rate from Ref. [14],  $\kappa = 2\pi \times 56$  kHz. The cavity addresses the  $D_2$  cycling transition of  $^{87}\text{Rb}$ , which is a  $\lambda = 780$  nm transition with a decay rate of  $\gamma = 2\pi \times 6.066$  MHz [15]. We

assume the injected field leads to a cavity pump rate  $\eta_0 = 2\pi \times 33$  MHz and is detuned from the atomic resonance by  $|\Delta_a| = 2\pi \times 50$  MHz. The cavity frequency is also far detuned from the atomic resonance, while being detuned from the pump's frequency by  $|\Delta_c| = 2\pi \times 5.1$  MHz. Since all frequencies are within  $O(100$  MHz) from one another, we approximate the wavenumbers  $k$  to be constant such that the recoil frequency from all photons in the system is approximated as  $\omega_r = 2\pi \times 3.77$  kHz [15].

With all of these specified experimental parameters, we obtain  $|U_0| = 2\pi \times 2.5$  kHz,  $|\Delta'_c| = 2\pi \times 4.85$  MHz, and  $|\beta_0| = 6.8$ . Furthermore, a drop time of  $\tau = 20$  ms leads to  $kg\tau = 2\pi \times 0.25$  MHz such that  $\omega_g = -2\pi \times 0.488$  MHz. This satisfies  $kg\tau \gg 2\omega_r$ , which was used in Eqs. (S29) and (S31), by a factor of 33. We thus have all of the needed quantities to simulate Eq. (S33). We can also calculate the perturbation  $|\epsilon| = 5.1 \times 10^{-4}$ , standing field  $|U_0||\beta_0|^2 = 2\pi \times 0.115$  MHz, and effective non-linear interaction rate  $|\chi_0| = 2\pi \times 59.2$  Hz such that  $N|\chi_0| = 2\pi \times 5.92$  kHz. We can now calculate ratios to check each of the approximations used in deriving Eq. (S33), which we present in Table. I. We find that all our approximations are satisfied by at least a factor of 10, while also satisfying  $|\Delta'_c| \gg \omega_g$  used in Eq. (S21) by a factor 10. We therefore expect our simulations of Eq. (S33) to be a realistic model of the current vertical cavity experiment of Ref. [14].

Approximation	Inequality ( $A \gg B$ )	Ratio ( $A/B$ )
Excited state elimination	$ \Delta_a  \gg \sqrt{N}\Lambda$	10
Cavity elimination	$ \Delta'_c  \gg N \chi_0 $	820
Cavity elimination	$ \Delta'_c  \gg  U_0  \beta_0 ^2$	42
Perturbation	$1 \gg N \epsilon /2$	39
Single momentum flips	$6kg\tau \gg  U_0  \beta_0 ^2$	13
Unwanted pair creation	$16\omega_r \gg N \chi_0 $	10

TABLE I. Table outlining the approximations assumed throughout the derivation as well as their corresponding ratios for our chosen experimental parameters.

- 
- [1] A. S. Holevo, in *Quantum Probability and Applications to the Quantum Theory of Irreversible Processes*, edited by L. Accardi, A. Frigerio, and V. Gorini (Springer Berlin Heidelberg, Berlin, Heidelberg, 1984) pp. 153–172.
- [2] D. W. Berry, *Adaptive Phase Measurements*, Ph.D. thesis, University of Queensland, Queensland (2001).
- [3] J. Combes and H. M. Wiseman, *Journal of Optics B: Quantum and Semiclassical Optics* **7**, 14 (2004).
- [4] L. Susskind and J. Glogower, *Physics Physique Fizika* **1**, 49 (1964).
- [5] D. W. Berry, B. L. Higgins, S. D. Bartlett, M. W. Mitchell, G. J. Pryde, and H. M. Wiseman, *Phys. Rev. A* **80**, 052114 (2009).
- [6] J. T. Reilly, S. B. Jäger, J. Cooper, and M. J. Holland, *Phys. Rev. A* **106**, 023703 (2022).
- [7] L. Pezzè, A. Smerzi, M. K. Oberthaler, R. Schmied, and P. Treutlein, *Rev. Mod. Phys.* **90**, 035005 (2018).
- [8] J. D. Wilson, C. Luo, J. T. Reilly, H. Zhang, A. Chu, A. M. Rey, M. J. Holland, and J. K. Thompson, *Momentum based entanglement in a vertical cavity* (2023), (to be published).
- [9] S. B. Jäger, T. Schmit, G. Morigi, M. J. Holland, and R. Betzholz, *Phys. Rev. Lett.* **129**, 063601 (2022).
- [10] I. Gradshteyn and I. Ryzhik, *Table of Integrals, Series, and Products*, 6th ed., edited by D. Zwillinger and A. Jeffrey (Elsevier Science, 2000).
- [11] A. Metelmann, O. Lanes, T. Chien, A. McDonald, M. Hatridge, and A. Clerk, arXiv preprint arXiv:2208.00024 (2022).
- [12] T. Holstein and H. Primakoff, *Phys. Rev.* **58**, 1098 (1940).
- [13] T. Byrnes and E. O. Ilo-Okeke, *Quantum atom optics:*

*Theory and applications to quantum technology* (Cambridge university press, 2021).

- [14] C. Luo, H. Zhang, V. P. Koh, J. D. Wilson, A. Chu, M. J. Holland, A. M. Rey, and J. K. Thompson, arXiv preprint arXiv:2304.01411 (2023).
- [15] D. A. Steck, Rubidium 87 d line data (2001).